Edinburgh Research Explorer

Operation Analysis of Thyristor Based Front-to-Front Active-Forced-Commutated Bridge DC Transformer in LCC and VSC Hybrid HVDC Networks

Operation Analysis of Thyristor Based Front-to-Front Active-Forced-Commutated Bridge DC Transformer in LCC and VSC Hybrid HVDC Networks

Peng Li, *Member*, *IEEE*, Grain P. Adam, *Member*, *IEEE*, Stephen J. Finney, Derrick Holliday

Abstract—The active-forced-commutated (AFC) bridge employs a symmetrical thyristor-bridge with auxiliary self-commutated full-bridge chain-link (FB-CL) circuit to assist its soft transition and forced commutation. This combination can form a thyristor based voltage source converter (VSC) with significantly reduced on-state losses and dc-fault blocking capability. Due to the full topological symmetry of the AFC-bridge, either current direction or dc-link voltage polarity can be reversed for power flow reversal as for the full-bridge modular multilevel converter (FB-MMC). Thus, the AFC-bridge is compatible with both line-commutated-converter (LCC) and VSC terminals in a multi-terminal high voltage direct current (MT-HVDC) network. This paper investigates its front-to-front (F2F) dc-dc application for matching the regional dc grids in a LCC and VSC hybrid HVDC network. Simulation studies are carried out to demonstrate its potentials as a high efficiency multi-functional solution for dc-dc conversion.

Index Terms—**Active-forced-commutated bridge, thyristor, IGBT, high efficiency VSC, front-to-front dc-dc converter, dc-link voltage reversal, LCC and VSC hybrid HVDC grid.**

I.   INTRODUCTION

With the development of high capacity voltage source converters (VSCs), the generic multi-terminal high voltage dc (MT-HVDC) grid with seamless power flow controllability (including power reversal) for each branch of its complex structure becomes possible [1-6]. VSC based networks can control the bidirectional power flow in a manner of changing the current direction while maintaining a nearly constant voltage.

Compared to VSC, conventional thyristor based line-commutated-converter (LCC) is usually configured as point-to-point connection due to its current source nature that needs to alter the dc-link voltage polarity for power reversal. It also suffers from the weaknesses of lacking reactive power control and ac grid strength dependency [6]. Nevertheless, LCC offers higher conversion efficiency and proven reliability up to ultra-high voltage (UHV) applications compared to the VSC solutions using self-commutated switches. Therefore, it remains dominant in the construction of large-scale converter station for UHVDC links [7-9]. The compensation strategies for improving the commutation and reactive power performances of LCC can be implemented by using controlled capacitors or VSCs [10-12].

In attempt to match the dc operating voltages in different parts of large regional dc grids directly rather than through the established ac network, the concept of dc transformer has been suggested and studied extensively. One of the most viable layouts for dc transformer is the isolated front-to-front (F2F) dc-dc converter, which originates from the dual-active-bridge (DAB) in medium voltage applications and can be extended easily to multi-port configurations, while preserving galvanic isolation [13-16]. For satisfying the requirements of HVDC systems, modular multilevel converter (MMC) using half-bridge (HB) chopper cell has been developed to reduce the switching losses and overcome the voltage level limit of using switch series connection as in the two-level VSC [17]; also, several variants of HB-MMC including hybrid topologies have been proposed in literatures, aiming for a compromise between the converter functionality and total energy storage [18-20]. These topologies can be configured as F2F dc-dc converters to meet most of the requirements in a MT-HVDC system such as the scalable structure, dc voltage tapping and galvanic isolation [21]. On the other hand, the non-isolated layouts for high voltage dc-dc conversion have also been studied in

[22-24], which are implemented using MMCs. However, considering the requirement of large-scale power transmission with multi-stage power conversion, the relatively high semiconductor loss is one of the major concerns for the development of dc transformer and other HVDC infrastructures.

Furthermore, the compatibility of all above VSC terminals with existing LCC stations falls apart during power reversal. This is because of inability of the HB cells or the directing switches in the aforementioned converter topologies to sustain reversed dc voltage as required by the LCC for changing its power flow direction. To overcome this issue, a VSC scheme that has complete topological symmetry is required to offer the ability of both current and voltage polarity reversal. One option that satisfies this requirement is to adopt the full-bridge (FB) cell in a MMC topology, which, by exploiting the positive and negative polarities of the cell output voltages, can fully control its ac side voltage (hence, current and power flow) under bipolar dc-link voltage [25]. However, the high investment and high power losses constrain the practical acceptance of FB-MMC at present [26, 27].

The active-forced-commutated (AFC) bridge has recently been proposed in [28] to establish a VSC scheme by using symmetrical thyristor-bridge as the main power paths and an insulated-gate bipolar transistor (IGBT) based FB cell chain-link (CL) for the controlled transition and forced commutation of main thyristors. With the assistance of FB-CL, AFC-bridge can fully control the turn-on and turn-off of its thyristors in a manner that allows elimination of operational dependency on the live ac network compared to conventional LCC. Moreover, AFC-bridge operates similarly as a typical VSC, offering two control degrees of freedom to regulate the magnitude and phase angle of its ac terminal voltage (reactive and active power). Both parts of this hybrid configuration are topologically symmetrical for current and voltage polarity, so it can block ac current infeed during a dc short-circuit fault, conduct bidirectional current and operate under bipolar dc voltage. Thus, AFC-bridge could be viewed as equivalent to a FB-MMC in terms of system-level functionalities but with similar or lower losses than HB-MMC due to the adoption of thyristors. Also, the voltage rating and total number of floating sub-module capacitors in the FB-CL of AFC-bridge is drastically reduced compared to MMC approaches. This, combined with the proven track record of thyristor technology

in UHVDC projects, offers reduced circuit complexity for the AFC-bridge with easier implementation of voltage level scale-up towards VSC based UHVDC systems.

The VSC nature of AFC-bridge is an essential difference compared to the combination of LCC with cascaded FB compensator that remains a current source nature in the main power circuit [12], making it suitable for developing the multi-terminal dc grid at reduced power losses [28]. This paper employs the AFC-bridge in a dc transformer to link both LCC and VSC terminals in a hybrid HVDC network. The reminder is organized as follows: section II briefly summarizes the key features of AFC-bridge and describes its F2F dc transformer configuration; in section III, the analysis and control strategy of F2F AFC-bridge dc-dc converter in a LCC and VSC hybrid HVDC network are interpreted; then, the intrinsic dc-fault blocking capability of AFC-bridge is discussed and a dc-fault protection strategy is proposed for its dc transformer configuration in section IV; simulation results are presented in section V; finally, the useful extensions and key observations are highlighted in section VI and VII.
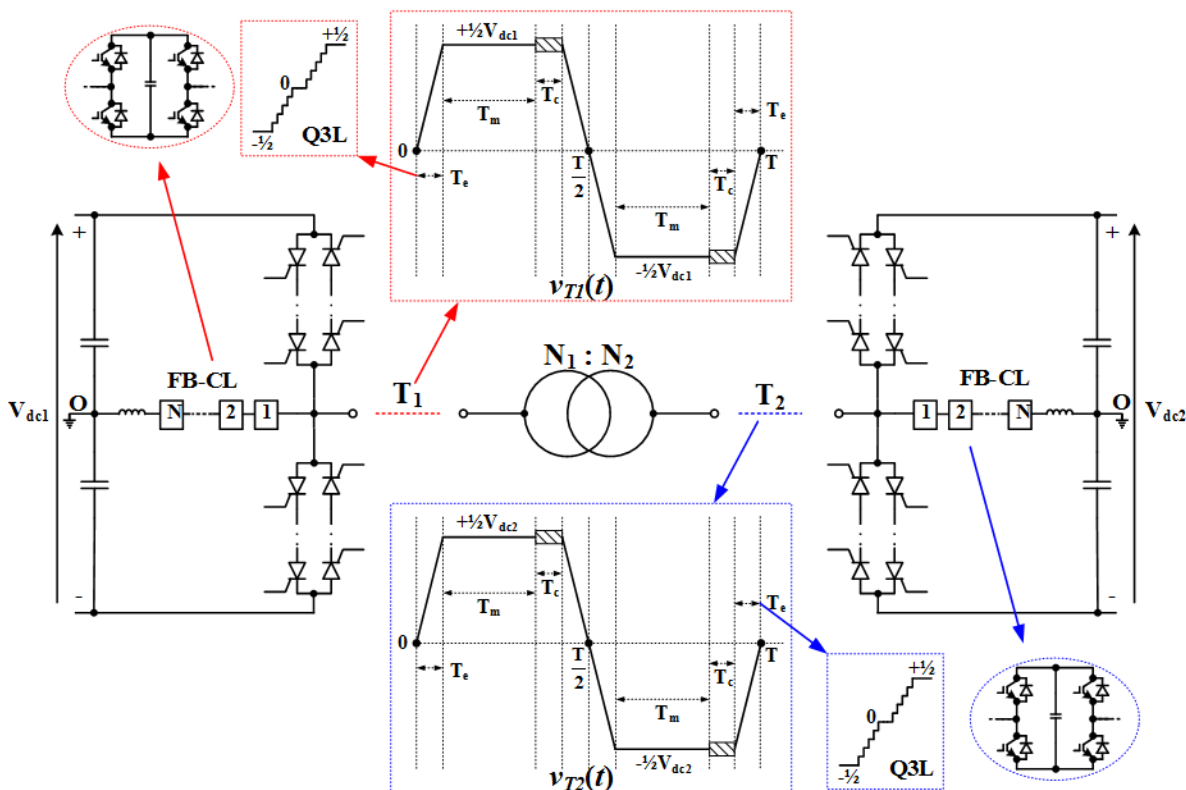
II. OPERATION LAW OF THE F2F AFC-BRIDGE

Fig. 1. AFC-bridge with fully controlled ac terminal voltage (decoupled active and reactive power control) within the ac-link of its F2F dc-dc configuration.

4

Fig. 1 clarifies the AFC-bridge topology and its ac terminal voltage in a F2F dc-dc configuration, where the ac-link can utilize both fundamental component and key harmonics of the trapezoidal voltage waveform to transfer power between each VSC terminal. The trapezoidal voltage waveform of each AFC-bridge is mainly composed of the voltage stepped transition period T_e (from 0 to either dc rail) produced by its FB-CL and the dc rail voltage clamping period T_m when one of the thyristors conducts. Particular, a thyristor forced turn-off period of T_c is facilitated by the internal redundant cells of the FB-CL with a net negative voltage across the previously conducted thyristor. As a result, the fundamental frequency of this trapezoidal voltage can be calculated by (1). Assuming an AFC-bridge with N_T cells to support the half dc-link voltage $\frac{1}{2}V_{dc}$ and N_c redundant cells to produce negative voltage across the thyristor ($N_c \ll N_T$), all cell capacitors in the FB-CL should have balanced voltage value V_u by a designed switching sequence considering the voltage sorting and current polarity; thus, (2) can be obtained. In the trapezoidal waveform, T_e is realized by switching a selected group of cells at each predefined instance with either even or uneven time steps, and the number of rotating cells at each time can be either equal or different provided the voltage gradients are lower than the maximum allowed dv/dt. In this manner, FB-CL offers various routes for the ac voltage of AFC-bridge to transit between zero and the two dc rails. Particularly, the zero-voltage-level with direct neutral-point-clamping (no charging or discharging burden on the floating capacitors) of the AFC-bridge can be employed as in Fig. 1 to form a quasi-3-level (Q3L) voltage that offers full range modulation index control at minimum commutation effort. In steady state, to achieve maximum efficiency for the AFC-bridge scheme, its ac voltage should have sufficiently high modulation depth, such that the zero-voltage-level duration is small enough and close to that for the intermediate voltage step dwelling time. If a basic linear slop transition with uniform time step T_d and one cell being switched per instance are assumed for steady state operation, (3) is obtained. Then, the ac side voltage of AFC-bridge under this case can be shown in (4), where t_0 is the zero-phase-angle instance, k is an arbitrary integer for each fundamental period, and $i_L(t)$ is the ac side load current that influences the cell voltage balancing and forced commutation scheme of the FB-CL.

$$f_o = \frac{1}{2 \cdot (2T_e + T_m + T_c)} \tag{1}$$

$$N_T \cdot V_u = \tfrac{1}{2} V_{dc} \tag{2}$$

$$N_T \cdot T_d = T_e \tag{3}$$

$$v_{TO}(t) = \begin{cases} \dfrac{V_{dc}}{2N_T} \cdot \text{round}(\dfrac{t - t_0 - k/f_o}{T_d}), & t \in [t_0 - N_T T_d + \dfrac{k}{f_o}, t_0 + N_T T_d + \dfrac{k}{f_o}) \\[2ex] \dfrac{V_{dc}}{2}, & t \in [t_0 + N_T T_d + \dfrac{k}{f_o}, t_0 + N_T T_d + T_m + \dfrac{k}{f_o}) \\[2ex] \dfrac{V_{dc}}{2} + \text{sgn}[i_L(t)] \cdot \dfrac{V_{dc} \cdot N_c}{2N_T}, & t \in [t_0 + N_T T_d + T_m + \dfrac{k}{f_o}, t_0 - N_T T_d + \dfrac{2k+1}{2f_o}) \\[2ex] -\dfrac{V_{dc}}{2N_T} \cdot \text{round}[\dfrac{t - t_0 - (2k+1)/(2f_o)}{T_d}], & t \in [t_0 - N_T T_d + \dfrac{2k+1}{2f_o}, t_0 + N_T T_d + \dfrac{2k+1}{2f_o}) \\[2ex] -\dfrac{V_{dc}}{2}, & t \in [t_0 + N_T T_d + \dfrac{2k+1}{2f_o}, t_0 + N_T T_d + T_m + \dfrac{2k+1}{2f_o}) \\[2ex] -\dfrac{V_{dc}}{2} + \text{sgn}[i_L(t)] \cdot \dfrac{V_{dc} \cdot N_c}{2N_T}, & t \in [t_0 + N_T T_d + T_m + \dfrac{2k+1}{2f_o}, t_0 - N_T T_d + \dfrac{k+1}{f_o}) \end{cases} \tag{4}$$

Detailed device-level analysis that influences the cell capacitor voltage balancing strategy and selection of passive components will be discussed in a separate device-oriented context; instead, this paper will focus on the system-level functionality of the AFC-bridge in a F2F dc transformer configuration for regional HVDC grids interoperability.

Taking terminal T_1 as an example, the ac-link voltage waveform mainly transits between two voltage levels of $\pm\tfrac{1}{2}V_{dc1}$ when the selected thyristor is in conduction state during each half cycle; while in voltage level transition periods, the FB-CL controls the waveform edge in a stepped transition manner to offer soft switching for the main thyristors and limit the *dv/dt* exerted on the ac-link transformer. Specially, when the thyristor needs to be turned off, the FB-CL will produce a negative net voltage across the on-state thyristor for its forced commutation. In this way, both turn-on and turn-off of thyristors in the AFC-bridge are fully controlled as in conventional VSCs. Since the majority of current is conducted by the thyristors in an AFC-bridge, its conduction loss profile can be largely improved compared to that for HB-MMC, combined with the extra gain of dc-fault reverse-blocking capability. Also, the FB-CL has no dc voltage and current stresses (in contrast to that for a MMC arm); and it only sustains about half dc-link voltage, requiring roughly quarter

amount of cells compared to MMC. This significant reduction on circuit complexity plus the use of thyristors can bring enhanced practical voltage scalability for the VSC-HVDC systems.

Similar as the basic two-level DAB that is with pure square wave ac-link terminal voltages, the F2F AFC-bridge in Fig. 1 controls the active power by varying the phase angle difference between two ac voltages. Also, by changing the voltage magnitude, the circulating reactive power within the ac-link is controllable. Such magnitude changes should be realized using low frequency modulation schemes in order to limit the total switching losses. For example, by manipulating the conduction time of the FB-CL and thyristors in the AFC-bridge, the Q3L ac voltage waveform with stepped level transition enables full range modulation index adjustment; thus, black-start capability is guaranteed for the AFC-bridge based converters. Alternatively, if zero-voltage-level is not exploited, a series of selective harmonic elimination (SHE) methods under a quasi-2-level (Q2L) mode can be adopted; but these incur either additional losses or high control complexity on fundamental voltage regulation over a wide range [21, 29]. The transformer link in the AFC-bridge dc-dc converter is possible to run with a frequency reasonably higher such as 100Hz (considering the speed of thyristors); in this manner, the overall size and weight of the converter can be reduced [30]. With phase-shift control, soft switching performances for the turn-on of self-commutated switches and turn-off of their anti-parallel diodes can be achieved for much of the operation range in traditional DAB, which is inherited by the FB-CL parts in the F2F AFC-bridge [15]. Also, the main thyristors undergoes nearly zero voltage switching (ZVS) with stepped voltage transition manner controlled by the FB-CLs [20, 28].

Recall the steady-state ac-link voltage of $v_{T1}(t)$ in Fig. 1. By ignoring the very short forced commutation period, it can be described by a standard trapezoidal waveform with a slope of $\frac{1}{2}V_{dc1}/T_e$. Then, the Fourier series of $v_{T1}(t)$ is obtained as in (5), where $\omega=2\pi f_o$ is the fundamental angular frequency used in the ac-link, and n is an odd integer for different order of harmonics. Then, if $v_{T2}(t)$ has a phase angle of δ relative to $v_{T1}(t)$, it can be expressed by (6), similarly. When $v_{T1}(t)$ leads $v_{T2}(t)$, the active power flows from dc port V_{dc1} to dc port V_{dc2}, and vice versa. Also, from (5) and (6), the dominant low order harmonic components of the ac-link voltages can also contribute to the active power transfer in a F2F dc-dc converter.

$$v_{T1}(t) = \frac{2V_{dc1}}{\pi} \cdot \sum_{n=1,3,5...} \frac{\sin(n\omega T_e) \cdot \sin(n\omega t)}{n^2 \omega T_e} \tag{5}$$

$$v_{T2}(t) = \frac{2V_{dc2}}{\pi} \cdot \sum_{n=1,3,5...} \frac{\sin(n\omega T_e) \cdot \sin(n\omega t + n\delta)}{n^2 \omega T_e} \tag{6}$$

It is noticed that the AFC-bridge topology is fully symmetrical; hence, besides of the bidirectional current conduction ability as in normal VSCs, it can also reverse the dc-link voltage polarity as in the FB-MMC but at much lower losses. This means that if the dc-link voltage is reversed (such as in a LCC system), the AFC-bridge can maintain its ac-link output voltage at the established operation point to continuously support the power flow regulation between other converter terminals.

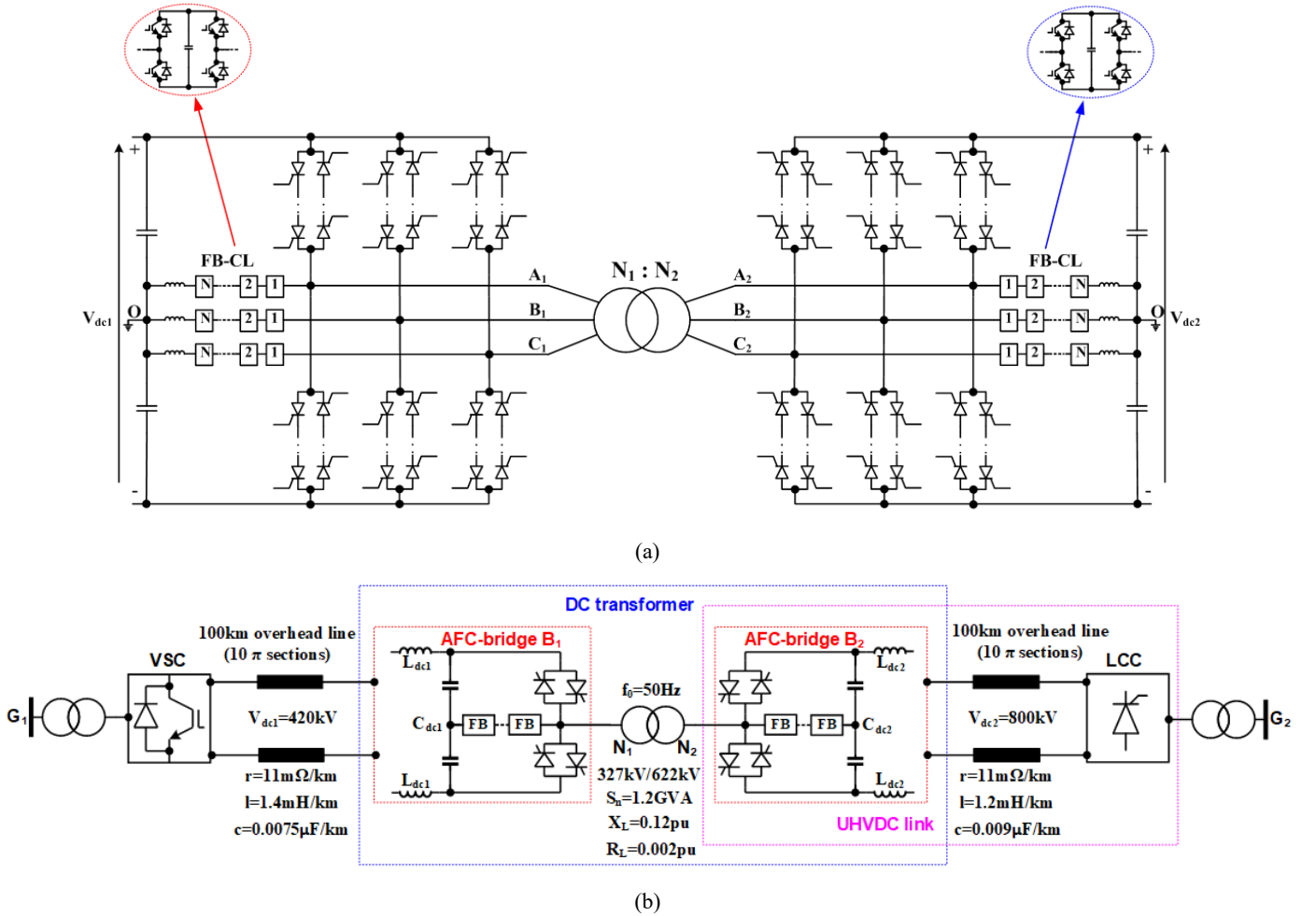## III.   F2F AFC-Bridge for Interoperability of LCC and VSC Terminals

(a)

(b)

Fig. 2. The configuration of studied system: (a) three-phase F2F AFC-bridge; (b) hybrid two-terminal HVDC grid with LCC and VSC stations linking via a F2F dc transformer using the AFC-bridge.

The topology of three-phase F2F AFC-bridge is described in Fig. 2(a), and Fig. 2(b) shows a hybrid two-terminal HVDC grid with both LCC and VSC stations linked via a F2F AFC-bridge dc transformer, in a symmetric monopolar arrangement. The 800kV UHVDC terminal B_2 is implemented by an AFC-bridge. Then, the dc transformer active bridge B_1 for matching the lower dc voltage port (420kV) can be built by either an AFC-bridge or a Q2L mode MMC; and particularly, the former is adopted in this study. The basic point-to-point system in Fig. 2(b) is employed in this paper to illustrate the operation laws and application details of the F2F AFC-bridge dc-dc converter; and its generic multi-terminal and bipolar configuration can be extended accordingly. Note that, in a F2F dc-dc converter, the potential use of ac-link frequency higher than the line frequency is able to reduce the overall size but also causes increased losses. The maximum ac-link frequency is also limited by the commutation time of the adopted thyristor. In this paper, the F2F AFC-bridge based dc transformer is operated with the ac-link frequency of f_o=50Hz.

In Fig. 2(b), when the LCC operates as a rectifier, the power flow is driven from the LCC station into the VSC area. During power reversal, the current of VSC and AFC-bridge B_1 ramps down and finally reverses its direction; while the LCC needs to shift into an inverter mode to change the voltage polarity of the UHVDC link. During the bipolar dc-link voltage that is determined by LCC, the AFC-bridge B_2 will alter its FB-CL output voltage and conduct its thyristor in opposite ways to retain the full range ac voltage synthesis ability. In this manner, the AFC-bridge is compatible with both VSC and LCC.

To control the power flow, the classical phase-shift scheme is adopted for the proposed dc transformer, where one of the bridge terminals (such as the lower voltage side AFC-bridge B_1) is employed to produce a voltage reference; and, through the isolated transformer, the voltage of the other terminal (such as the UHVDC side AFC-bridge B_2) is regulated around this reference with either leading or lagging phase angle to initiate the demanded power flow. Additionally, if the dc-link voltage is selected as control target, the phase-shift angle of two bridges can also be used to change the voltage tapping ratio of the dc transformer [13, 31]. Within this paper, only the phase-shift control is utilized for the F2F AFC-bridge dc transformer to control the power flow between two regional dc grids; while no ac voltage magnitude control is involved for controlling the reactive power circulation in the ac-link [16]. Hence, the steady state outer-layer controller of

F2F AFC-bridge dc transformer in Fig. 2(b) can be described in Fig. 3, where the outer-layer proportional-integrate (PI) controller produces the phase-shift angle in relative to the ac voltage v_{T1}; also, an inner current compensator C_i can be used to improve the dynamic response and correct the ac-link current that may be influenced by unbalanced line inductances practically. When active power transfer is not required in an AFC-bridge, its thyristors can be disabled, such that the associated FB-CL is capable of supporting the ac side voltage continuously with reactive power control.
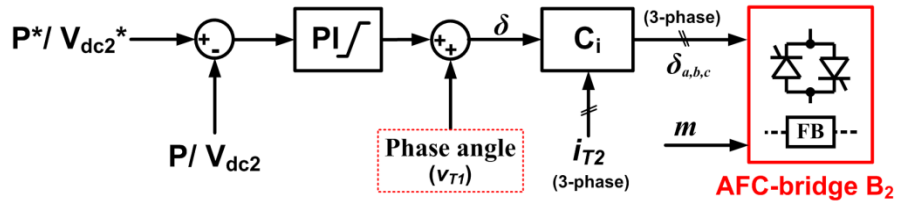

Fig. 3. Generic control strategy for power flow (dc voltage) control of the F2F AFC-bridge dc transformer.

With these observations, the power flow reversal sequence of the LCC and VSC hybrid network in Fig. 2(b) can be described as follows:

- At first, the dc transformer reduces the active power from the initial value gradually to zero using the phase-shift scheme in Fig. 3.

- Then, the UHVDC-link voltage starts to reverse by adjusting the valve firing angle of LCC; and during this process, the FB-CL of the AFC-bridge is able to support the previous ac voltage with pure reactive power exchange (internal losses are neglected).

- Once the LCC dc voltage is totally reversed to reach the nominal magnitude, the full active power control functionality of the AFC-bridge is enabled again and its thyristors will be resumed to operate as the main power paths.

- After dc voltage polarity is changed, the power flow command in Fig. 3 transits from zero to an opposite-sign value to establish the reversed power flow.

In summary, by adopting symmetrical thyristors in the main power paths, AFC-bridge VSC achieves low conversion losses, enhanced voltage scalability and bipolar dc voltage operability; hence, it can serve as an interface to integrate the LCC stations into VSC based HVDC grid with bidirectional power flow capability.

IV.   DC-FAULT PROTECTION OF AFC-BRIDGE DC TRANSFORMER

For the concept of future dc grids, the dc fault management is a major concern in practice. The two-level VSC and HB-MMC will absorb very high uncontrolled rectification current through their anti-parallel diodes when dc-link voltage falls below the peak ac line voltage. As a result, if these converters are connected to a strong ac grid, the dc circuit breaker (CB) is required to isolate the fault section rapidly [32]. Several reverse-blocking topologies such as FB and mixed cell MMCs have been proposed to offer internal dc-fault tolerance [33, 34]. Nonetheless, these solutions increase the total number of switching devices and cause higher power losses, making them less attractive in practical applications.

The AFC-bridge eliminates any uncontrolled diode path by the hybrid use of symmetrical thyristor-bridge and reverse-blocking FB-CL circuit. During a dc-fault, the thyristor in conduction mode will be turned off by its associated FB-CL before dc-link voltage drops down to a certain level; afterwards, FB-CL is able to fully and rapidly decay the ac current infeed. Alternatively, the reverse-bias of on-state thyristors can depend on the ac grid voltage, in a similar way of conventional LCC; while the FB-CL only protects itself with reduced dynamic rating burden on its cell capacitors. Importantly, this dc-fault blocking feature of AFC-bridge is achieved without sacrifice on the efficiency performance in contrast to a FB or mixed cell MMC; rather, it operates the low loss, low cost and robust thyristors as close as possible to a standard VSC, which further reduces the losses of HB-MMC and retains its key control flexibility [28]. Additionally, the semiconductor area and total cost of AFC-bridge are advantageous, considering that its total amount of cell capacitors and number of IGBTs (more expensive than thyristors) are significantly smaller than in a MMC, not to mention the protective thyristors installed in each cell of HB-MMC for over-current bypass [35].

Beyond the discussions on dc-fault isolation of grid-connected converters, special considerations can be taken for the dc-dc arrangements, where devices are exposed to weak ac network in the transformer. For a

HB-MMC dc transformer without dc CB, the dc-fault propagation can be prevented by blocking all converter terminals to deprive the ac infeed. On the other hand, the use of reverse-blocking topologies (such as FB or mixed cell MMC) in a generic MT-HVDC grid enables flexible and rapid isolation of faulty parts without interruption on power transfer between healthy terminals (except for some level of power oscillation). Note that the AFC-bridge can operate equivalently to a typical reverse-blocking converter by promptly triggering its FB-CL to cut off the thyristor path during dc-fault protection.

Compared to the above two cases (HB-MMC and self-blocking converters), the proposed dc-fault ride-through strategy in this paper for the AFC-bridge based dc transformer enjoys somewhere in between; and it can reduce the requirement on the FB cell capacitors. In this scheme, once a dc-fault is affirmed, the gate signals of faulty side thyristors and FB-CLs will be blocked; and the healthy terminals continue running to supply the ac-link voltage for the thyristor recovery. In such method, the FB-CL current can decay rapidly; while if any rectifier mode thyristor of the faulty terminal is previously in conduction state, it will be turned off (reverse-biased) by the ac network voltage. The possible ac infeed fault current paths through the rectifier mode thyristors of an AFC-bridge are shown in Fig. 4(a). Specially, to accelerate the reverse bias of on-state thyristors and reduce the recovery current level, the healthy terminals of AFC-bridges should transit into an increased ac-link frequency f_H for a very short period as in Fig. 4(b), which can effectively increase the ac line impedance and limit the fault current level to be compatible with the relatively low surge current capability of IGBT. Then, the healthy converters will resume the frequency back to normal. During this frequency jump process, since the energy stored in the FB cell capacitors can support the power flow for a short duration, the thyristors of healthy AFC-bridge terminals can be activated or inactivated; and the value of increased frequency f_H is selected considering the peak current level and the thyristor commutation time; such that inequality (7) must be satisfied, where V_{pk} represents the peak value of ac voltage, L_T includes the total inductance of the current loop in Fig. 4(a), and I_{CN} is the current rating of the employed IGBT device.

$$\begin{cases} \dfrac{V_{pk}}{2\pi \cdot f_H \cdot L_T} < I_{CN} \\ 2 \cdot (T_c + T_e) < \dfrac{1}{f_H} \end{cases} \tag{7}$$
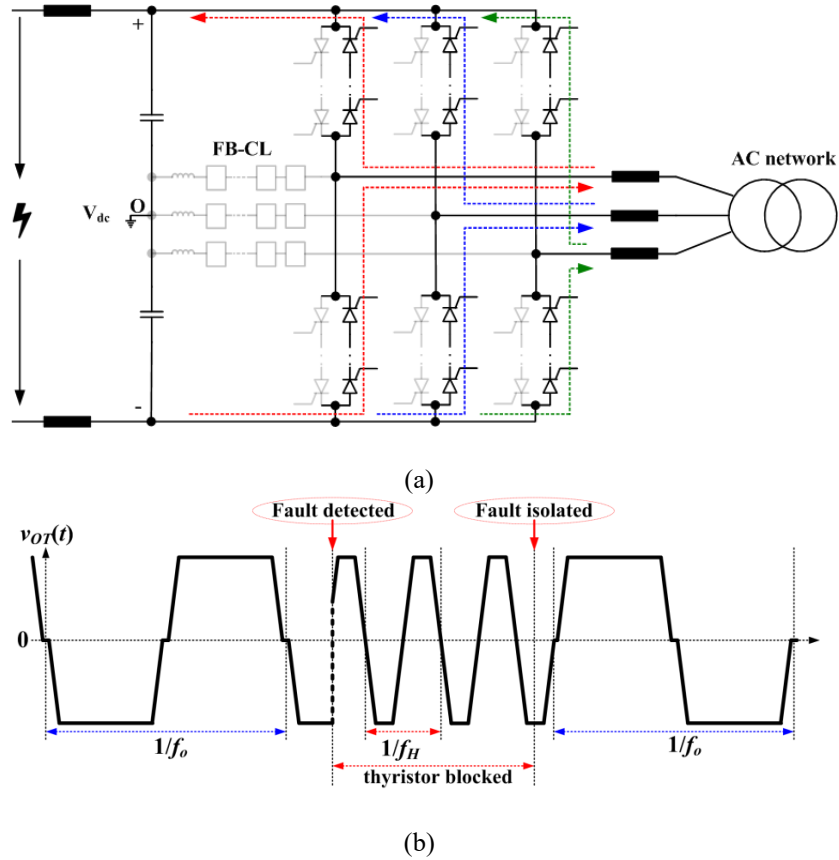
(a)

(b)

Fig. 4. The proposed dc-fault isolation of AFC-bridge dc transformer: (a) possible thyristor paths for ac infeed of fault current after FB-CLs are blocked; (b) frequency jump of the ac-link voltage for healthy terminals during dc-fault protection.

   With the proposed dc-fault protection strategy, the healthy AFC-bridge terminals in a multi-port dc-dc configuration can maintain full power transfer capability among each other but only with a very short period of frequency jump operation to assist the isolation of faulty converters. Since the FB-CL retains full energy in its cell capacitors, the blocked AFC-bridge can repossess full functionalities rapidly once fault is cleared.

   Although the dc-fault protection strategy in Fig. 4(b) is more valuable for multi-terminal configurations, the point-to-point system in Fig. 2(b) is sufficient for the simulation study in later section to demonstrate the rapid blocking of only the faulty side AFC-bridge. At the same time, it is worth mentioning that the proposed frequency jump approach may also be viable in a HB-MMC multi-terminal dc transformer to increase the ac line impedance temporarily (for example, 40ms); thus, allowing enough time for the sole use of ac CB to trip the fault before the infeed current rises to a destructive level.

V. SIMULATION STUDY

In the studied system of Fig. 2(b), the VSC and LCC terminals are operated in dc voltage control mode and matched by the AFC-bridge dc transformer. Through overhead power lines, the VSC station is connected with 420kV lower voltage side AFC-bridge B_1, and an 800kV UHVDC link integrates the LCC and AFC-bridge B_2; thus, forming a symmetric monopolar system. The power line impedance near each AFC-bridge is modeled as a local inductance; and a dc capacitance is installed and split to give the access to the neutral point for connecting the FB-CL. In this system-oriented context, 11 FB cells are used in each FB-CL to accelerate the simulation; and 10 of them are responsible for sustaining the half dc-link voltage.

TABLE I. Key parameters of the simulation study.

AFC-bridge B_1	
dc-link voltage V_{dc1}	420kV
local line inductance L_{dc1}	1mH
dc-link capacitance C_{dc1}	120μF
FB-CL cell number	11 (N_T=10, N_c=1)
FB cell capacitance	960μF
FB-CL inductance	7.5mH
Overhead line between VSC and AFC-bridge B_1	
length	100km
resistance	11mΩ/km
inductance	1.4mH/km
capacitance	0.0075μF/km
PI section number	10
AFC-bridge B_2	
UHVDC-link voltage V_{dc2}	800kV
local line inductance L_{dc2}	0.5mH
dc-link capacitance C_{dc2}	30μF
FB-CL cell number	11 (N_T=10, N_c=1)
FB cell capacitance	240μF
FB-CL inductance	15mH
Overhead line between LCC and AFC-bridge B_2	
length	100km
resistance	11mΩ/km
inductance	1.2mH/km
capacitance	0.009μF/km
PI section number	10
LCC dc smoothing inductance	270mH
Transformer in the ac-link	
apparent power rating S_n	1.2GVA
fundamental frequency f_o	50Hz
voltage ratings N_1:N_2	327kV/622kV
leakage impedance R_L+jX_L	0.002pu+j0.12pu

The key parameters used for simulation study of Fig. 2(b) are summarized in TABLE I, and two cases of F2F AFC-bridge dc transformer are investigated, both under normal operation and dc short-circuit fault. In this simulation studied, the three-phase transformer leakage inductances are set to be balanced; hence, the current compensator C_i in Fig. 3 is not activated.

A. Power Flow Control Under Normal Operation

The first simulation case for the model of Fig. 2(b) is carried out under normal operation to validate its bidirectional power flow control capability.

With the power direction from the LCC (AFC-bridge B_2) to the VSC (AFC-bridge B_1) chose as positive, Fig. 5 records the bidirectional power flow response and key waveforms of AFC-bridge B_2. Initially, a total power flow of 180MW is transmitted from the UHVDC-link V_{dc2} to the lower dc port V_{dc1}; and the power reference starts to ramp up to 960MW from 0.1s to 0.3s. Then, at 0.5s, the power flow supplied by LCC terminal begins to decrease and reaches zero eventually. Staying at zero power status, the LCC dc-link voltage V_{dc2} will change its polarity to allow the power flow reversal. Afterwards, the command of power flow starts to decrease along the negative direction from 1s and stay at -960MW after 1.4s. Fig. 5(a) displays the power response of the tested dc transformer system; and the polarity reversal of UHVDC voltage V_{dc2} is shown in Fig. 5(b). Observe that the AFC-bridge B_2 can operate normally with bipolarity of V_{dc2}; and its current remains unidirectional during the power reversal of LCC station as in Fig. 5(c); while AFC-bridge B_1 connects to a VSC station and changes its current direction to reverse the power, see Fig. 5(d) (dc voltage of B_1 maintained constant as in conventional VSC). Also, the three-phase terminal voltage and output current transient of AFC-bridge B_2 are displayed in Fig. 5(e) and (f), which are zoomed in by Fig. 5(g) and (h). Thus, the AFC-bridge can run harmoniously with both LCC and VSC.
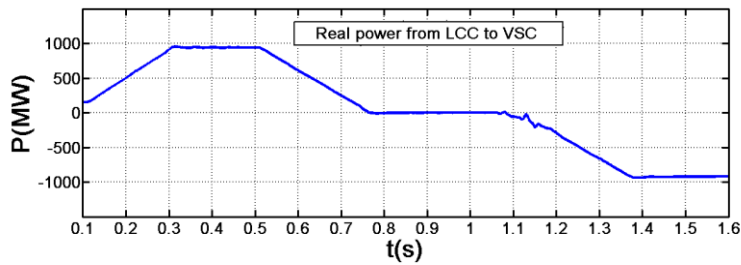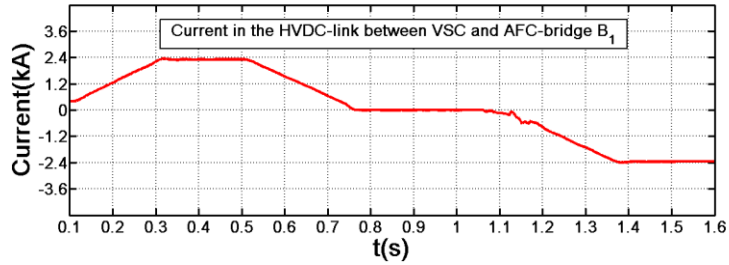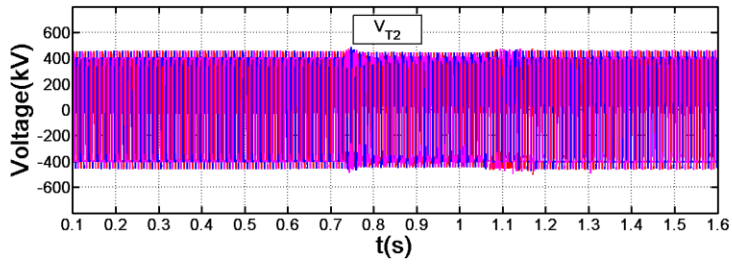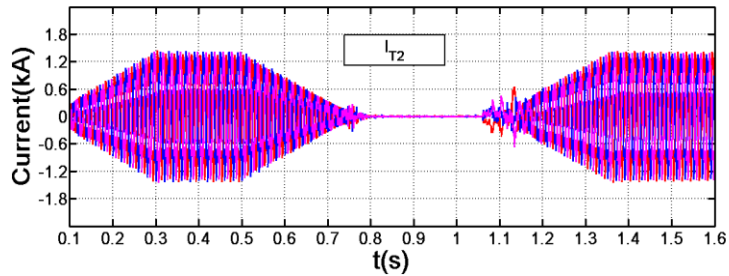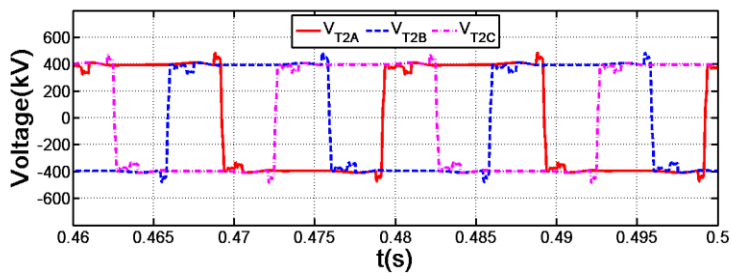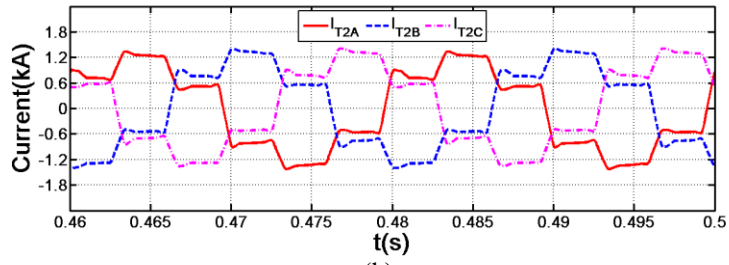

(a)
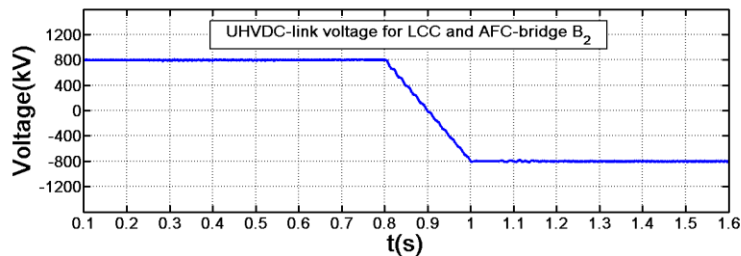
(b)
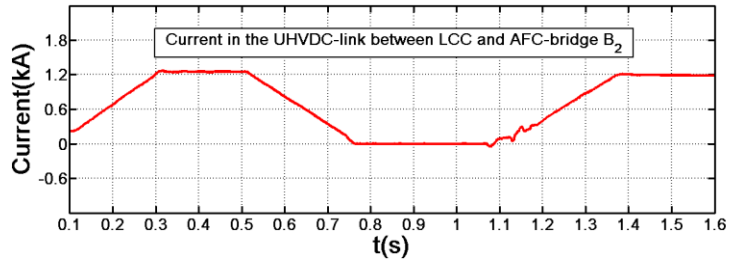
(c)

(d)

(e)

(f)

(g)

(h)

Fig. 5. The power flow response and key waveforms of AFC-bridge B_2: (a) transient response of power flow; (b) voltage reversal of UHVDC-link; (c) current of UHVDC-link; (d) current of VSC-HVDC-link; (e) ac terminal voltage transient of B_2; (f) output current transient of B_2; (g) zoomed-in three-phase terminal voltage of B_2; (h) zoomed-in three-phase output current of B_2.

In further, when power flow is positive (from LCC to VSC), Fig. 6 demonstrates the detailed waveforms of F2F AFC-bridge dc transformer in phase A. The ac terminal voltage of B_2 is in leading phase with that of B_1 as in Fig. 6(a); and the consequent output current of AFC-bridge B_2 can be obtained in Fig. 6(b), which is further distributed between its thyristors and FB-CL as in Fig. 6(c) and (d). Observe that the majority of the ac side current is carried by low loss thyristor paths; thus, the conduction losses can be significantly reduced in the AFC-bridge; and the overlap conduction period is used for thyristor commutation and energy exchange between the FB-CL and dc-link. Fig. 6(e) shows the FB cell capacitor voltage balancing results.
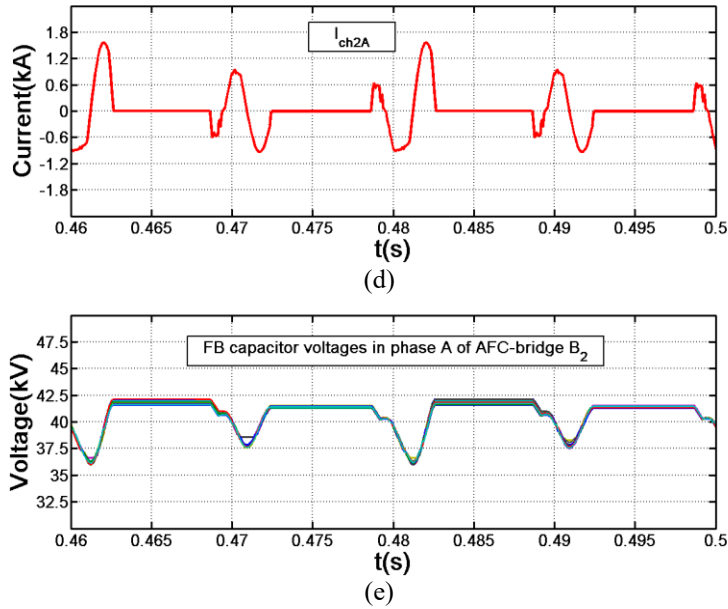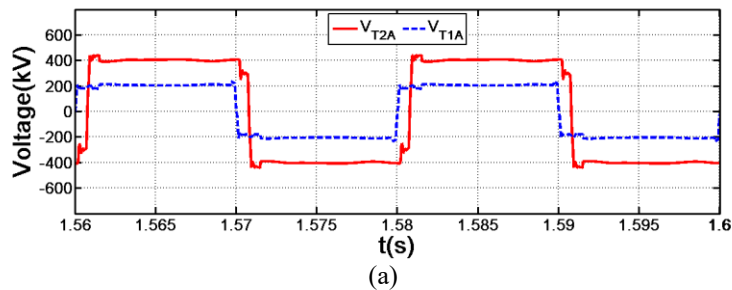

17

(d)

(e)
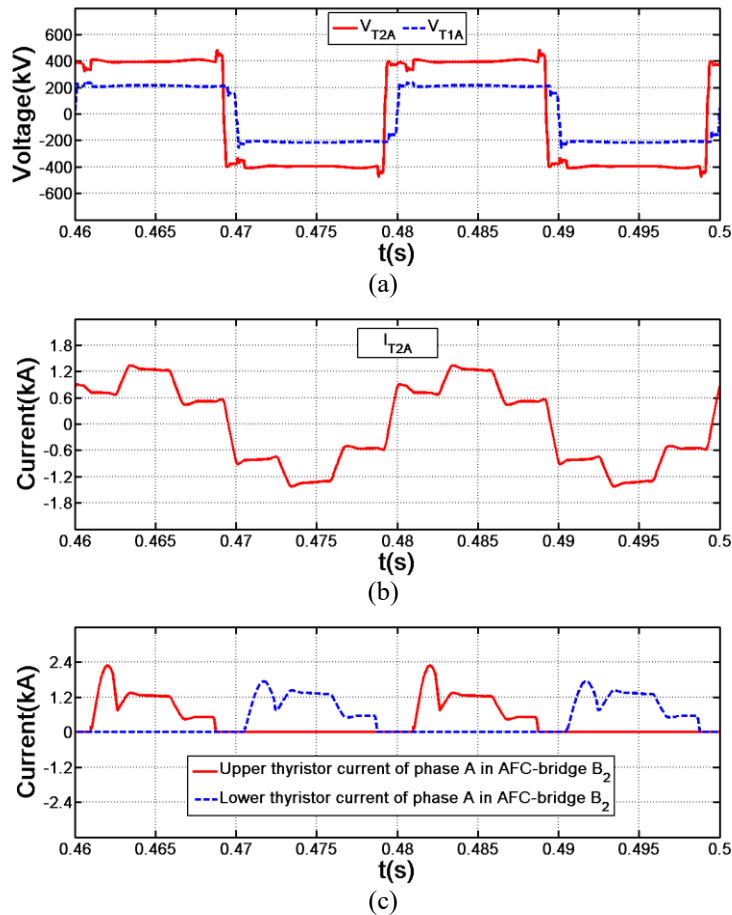
Fig. 6. Detailed waveforms of the F2F AFC-bridge dc transformer in phase 'A' with positive power flow from LCC to VSC: (a) ac terminal voltages of B_1 and B_2 with phase-shift; (b) ac output current of B_2 that connected to LCC; (c) current carried by thyristors of B_2; (d) FB-CL current of B_2; (e) FB cell capacitor voltages of B_2.

Similarly, if the power is sourced from the VSC area to the LCC (negative direction), the UHVDC voltage V_{dc2} needs to be reversed; while the ac terminal voltage of B_2 can be maintained stable with only its phase angle being adjusted to lag that of B_1 in order to drive the negative power flow. Fig. 7 summarizes the detailed converter-level results of F2F AFC-bridge under this case. Notice that, due to the high power factors of VSC terminals in a typical F2F dc transformer, the AFC-bridge B_2 connected to the LCC conducts majority of its output current through a fixed pair of thyristors under either power flow direction. Thus, its anti-parallel devices are low power-rated to handle only small amount of circulating reactive power, which can save the total cost. This is due to the fixed current direction determined by the LCC.
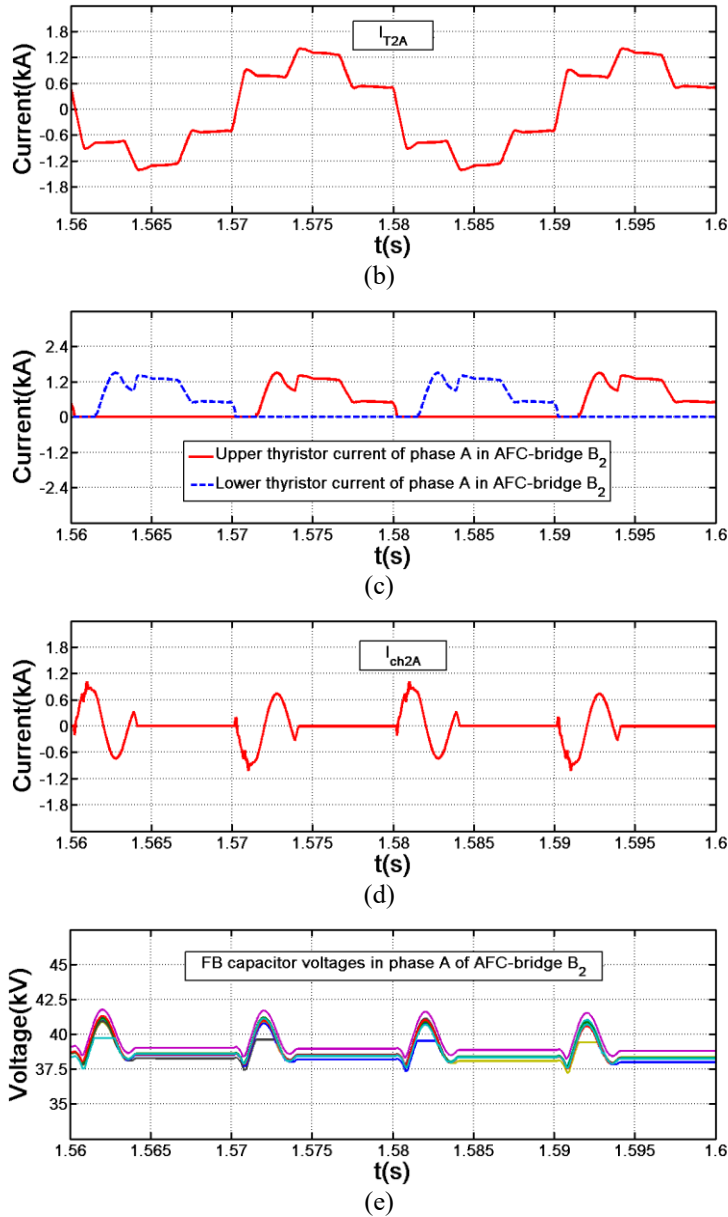

(a)

18

Fig. 7. Detailed waveforms of the F2F AFC-bridge dc transformer in phase 'A' with negative power flow from VSC to LCC: (a) ac terminal voltages of B_1 and B_2 with phase-shift; (b) ac output current of B_2 that connected to LCC; (c) current carried by thyristors of B_2; (d) FB-CL current of B_2; (e) FB cell capacitor voltages of B_2.

For AFC-bridge B_1 that is connected to the VSC station, it conducts the active power part of the ac current through either a certain pair of thyristors or their anti-parallel paths according to the power flow direction, which is the same as a standard VSC. For example, if B_1 absorbs power from the UHVDC-link (B_2 and LCC), it works as a load side rectifier using its anti-parallel thyristors to transmit power into the VSC station in Fig. 2(b). Alternatively, when the power flow direction reverses, B_1 will shift into an inverter mode with opposite current distribution among the symmetrical thyristors [28].

B. DC-Fault Ride-through Strategy

To validate the dc-fault protection scheme in Fig. 4(b). the second run of the simulation model assumes a dc fault (with 1Ω short circuit resistance) happens to the lower side dc-link voltage V_{dc1}, 5km away from the AFC-bridge B_1. The VSC station is modeled with dc-fault protection.

As shown by Fig. 8(a) and (b), the power flow (from LCC to VSC) ramps up from initial power 180MW to 960MW under normal dc-link voltage. At 0.8s, the dc short-circuit fault occurs; and the power flow drops to zero rapidly since no active power can be transmitted to a zero-voltage port. Then, assuming the fault is cleared at 0.9s, V_{dc1} starts to be recharged. After the nominal dc voltage level is resumed at 1s shown in Fig. 8(a), the power flow in Fig. 8(b) gradually restored to the rated level. During above processes, the ac-link current transient response of the F2F AFC-bridge (reflected to B_2 side) is displayed in Fig. 8(c); and its zoomed-in version around fault blocking period is given by Fig. 8(d), where, in order to reduce the recovery time of thyristors and limit the fault current, the healthy terminal B_2 has its ac voltage jump to 400Hz for 5ms and resume to 50Hz afterwards, see Fig. 8(e). Note that, if other healthy terminals are connected as for the case of a MT-HVDC network, the AFC-bridge B_2 can continue transferring power without interruption. The FB-CLs of faulty terminal B_1 are blocked to retain the cell capacitor energy in this simulation case.
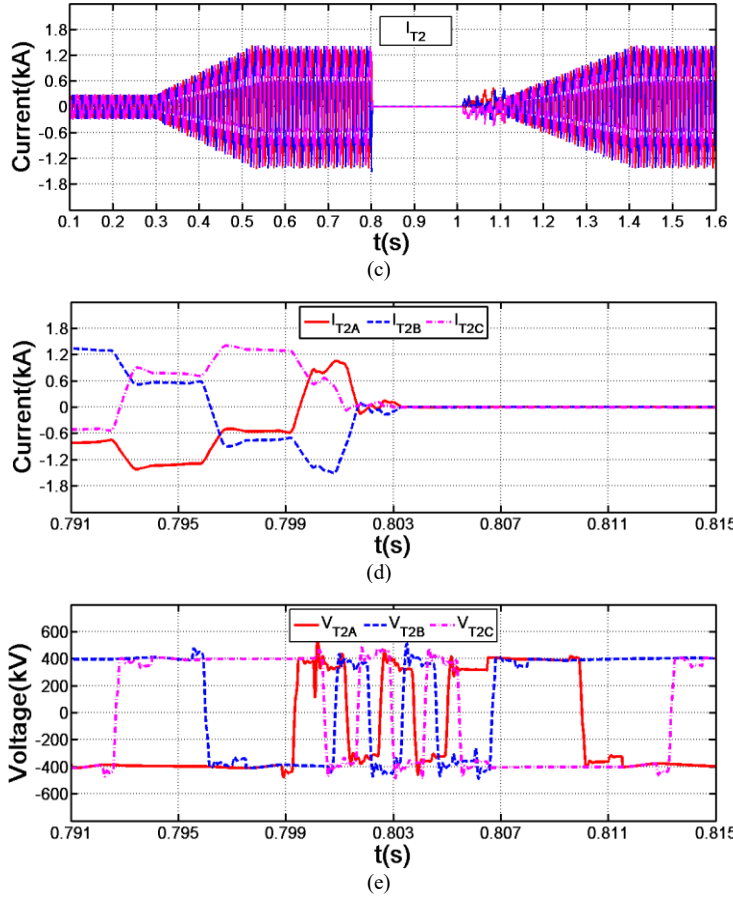

(a)

(b)
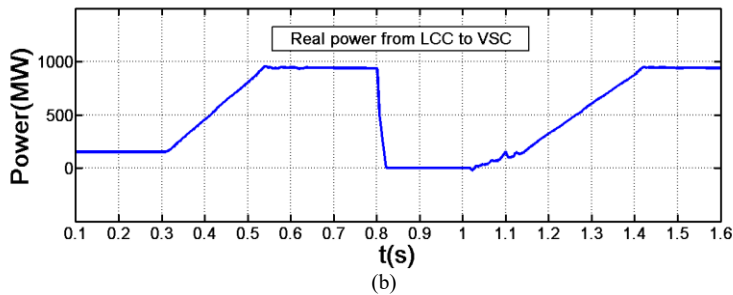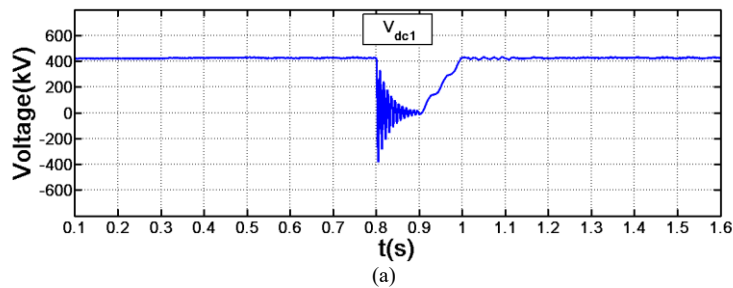
Fig. 8. Results for dc-fault ride-through and restoration of the F2F AFC-bridge: (a) dc-link voltage V_{dc1} of AFC-bridge B_1; (b) transient response of the power flow; (c) transient response of ac-link current reflected in B_2 side; (d) zoomed-in ac current of B_2 during dc-fault blocking; (e) ac voltage frequency-jump of healthy terminal B_2 during fault isolation.

In further, Fig. 9 shows the detailed waveforms of the F2F AFC-bridge in phase B during the dc-fault blocking period. The zoomed-in ac voltage response of healthy terminal B_2 is given in Fig. 9(a). With the frequency-jump operation of B_2, the on-state thyristor of the blocked AFC-bridge B_1 can be turned off rapidly as shown in Fig. 9(b) without significant over-current to protect the IGBT circuits. In Fig. 9(c) and (d), the FB-CL of B_1 is also blocked to create an open-circuit and decay the current rapidly; such that its cell capacitor voltages receive a certain level of charge-up and remain stable after ac current is fully cut off.
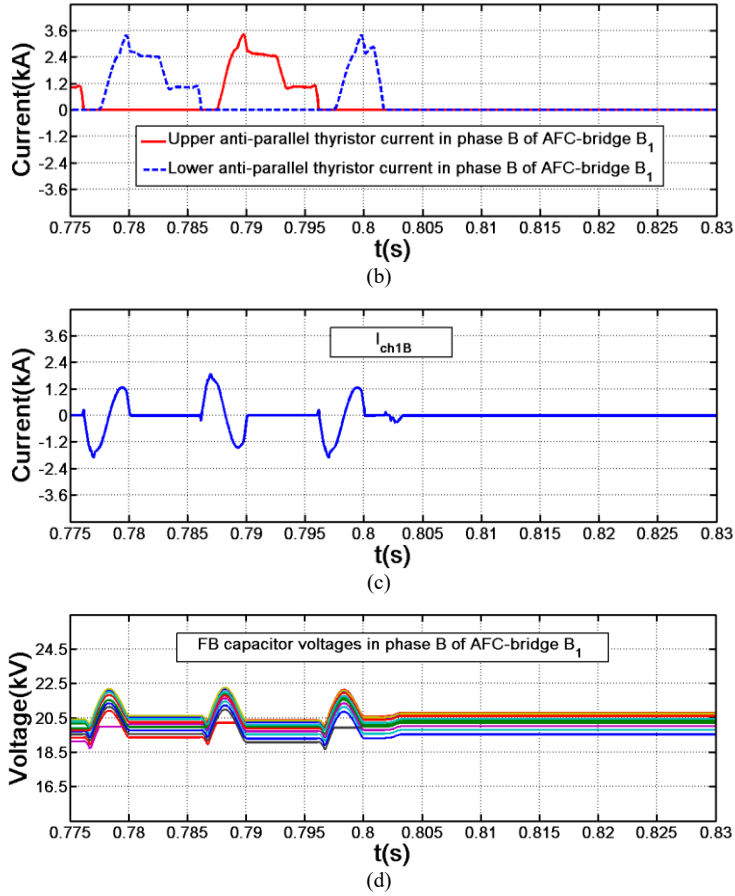

21
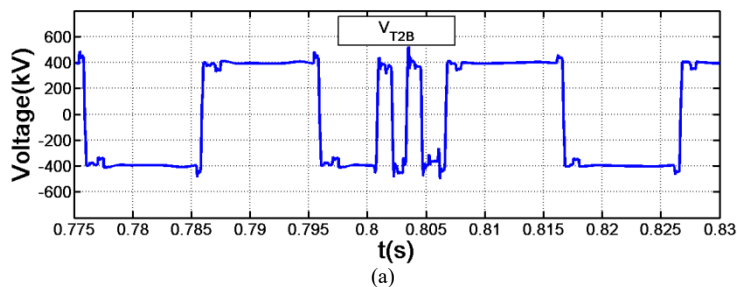
Fig. 9. Detailed waveforms of the F2F AFC-bridge in phase B during dc-fault isolation: (a) ac voltage of healthy terminal B_2; (b) turn-off of anti-parallel thyristor in faulty terminal B_1; (c) FB-CL current of B_1; (d) cell capacitor voltage of B_1.

VI.   DISCUSSIONS

TABLE II. The case study of semiconductor losses in AFC-bridge and HB-MMC with on-line calculation.

One three-phase converter terminal with 420kV dc voltage and 840MW output power			
Topology	Conduction losses	Switching losses	Total losses
AFC-bridge	2.391MW (0.285%)	2.258MW (0.269%)	4.649MW (0.553%)
HB-MMC	4.841MW (0.576%)	2.046MW (0.244%)	6.887MW (0.820%)

In an attempt to briefly assess the semiconductor losses of AFC-bridge and justify its suitability for HVDC applications, the 4.5kV IGBT T1800GB45A and 4.8kV thyristor T1551N are assumed to build the AFC-bridge terminal B_1 in Fig. 2(b); and the same IGBT is employed to construct a HB-MMC with same dc-link voltage and power rating. The loss calculation for both cases are carried out in a numerical simulation as given in TABLE II, which shows that the total semiconductor losses of AFC-bridge are significantly reduced by adopting thyristors in the main power paths. Practically, these power loss figures will be influenced by the

22

switching device utilization, tolerance band of voltage ripple for selecting cell capacitance, voltage balancing strategy and converter operation point.

Then, a high-level comparison between several promising VSC converters for HVDC applications are carried out under a fixed dc-link voltage of V_{dc} in TABLE III. For indication purpose, all switching devices are operated at the same voltage rating, and N of them can sustain the full dc voltage (N is chosen as an even integer). This comparison focuses on the device count, losses, footprint and system-level functionalities, covering the HB-MMC, FB-MMC, alternate arm converter (AAC) and AFC-bridge [18, 28, 33]. In the FB-CL of AFC-bridge, extra 10% sub-modules are assumed for the negative voltage injection across its main thyristors; and no backup cells for fault-bypass are considered in all these converters. Note that all estimated number of components in TABLE III need to be rounded up to have practical meanings; such that the actual device utilization will vary marginally. For the semiconductor losses and total capacitance requirement, the suggested ranges or case studies are supplied as these figures are highly depended on design specifications.

TABLE III. Comparisons for the key features required by a HVDC system between the AFC-bridge and other promising options.

	HB-MMC	FB-MMC	AAC in [18]	AFC-bridge
No. of cell capacitors (three phases)	N×6	N×6	½N×(1+27%)×6	½N×(1+10%)×3
DC-link capacitor (three-phase system)	no dc-link capacitor	no dc-link capacitor	dc-link buffer capacitor	dc-link buffer capacitor
No. of IGBTs (three phases)	2N×6	4N×6	3.04N ×6	2.2N×3
No. of thyristors (three phases)	usually, a minimum number of N×6 is needed for fault protection	none	none	N×6
No. of switches in the conduction paths (three phases)	N×6	2N×6	1.77N ×3 for the majority of a fundamental period	N×3 for the majority of a fundamental period
Estimated current stress for main power switches	half load current plus dc circulating current for capacitor energy balancing	half load current plus dc circulating current for capacitor energy balancing	load current plus dc side current for capacitor energy balancing	load current plus dc side current for capacitor energy balancing
Type of switches in normal conduction paths	IGBT	IGBT	IGBT	thyristor and IGBT
Semiconductor losses at rated power level	in the range of 0.64%~1% as suggested by [17, 36]; 0.820% in the case study of TABLE II	in the range of 1.3~2.35% as suggested by [36, 37]	>1% as suggested by [18, 27, 37]	0.553% in the case study of TABLE II
Total capacitance (assessed by converter energy density)	30~40KJ/MVA as suggested by [38]	35kJ/MVA in the case study of [26]	20.55kJ/MVA in the case study of [18]	16.6kJ/MVA in the case study of TABLE I
No. of limb inductors (three phases)	six	six	six	three
DC-fault blocking ability	no	yes	yes	yes
DC-link voltage	positive	bipolar	positive	bipolar

It is observed from TABLE III that the AFC-bridge offers following key advantages for building high voltage high power capacity converters:

- The AFC-bridge has roughly quarter number of cells (floating capacitors) compared to MMC, and half of that for AAC;

- As an indication of the conduction losses, the conduction path device number in the AFC-bridge is similar as HB-MMC and lower than that for other converters; also by carrying the main power through thyristors, it is expected to achieve a very low overall losses;

- All converters being considered are able to produce stepped transition waveforms for their ac side voltages (either sinusoidal type or trapezoidal type); hence, exerting low and controllable dv/dt on the interfacing transformer;

- The FB-CL part of AFC-bridge sustains only about half dc-link voltage; also, thyristors are very reliable and have proven track record for direct series-connection in UHVDC applications. As a result, its practical voltage scalability can be enhanced and has the potential to enable the use of VSC in UHVDC systems;

- Similar as for a FB-MMC, the AFC-bridge can work harmoniously with the LCC stations under bipolar dc-link voltage for bidirectional power flow;

- The system level functionalities of AFC-bridge are almost equivalent to those for a FB-MMC; but with similar (if not lower) overall losses than the HB-MMC, which is achieved by successfully operating the thyristor-bridge as a VSC.

VII.   CONCLUSIONS

In this paper, the active-forced-commutated (AFC) bridge is investigated under a front-to-front (F2F) dc transformer context for HVDC applications. Thanks to the use of thyristor as main power devices, the overall efficiency of an AFC-bridge can be significantly improved. As a VSC, it also offers intrinsic bipolar dc-link

voltage operability, dc-fault reverse-blocking capability and enhanced practical voltage scalability (reduced complexity and cost compared to MMC).

With the VSC nature of AFC-bridge, the two terminals in its F2F dc-dc configuration form the classical DAB scenario with full control on its real power flow and ac-link circulating current. Considering the two-stage power conversion layout in a F2F dc transformer, the use of AFC-bridge with reduced losses becomes even more attractive. In further, the AFC-bridge based solution is able to interconnect both VSCs and LCCs with bidirectional power flow. Due to the elimination of uncontrolled diode paths in each AFC-bridge, its dc-fault ride-through performance can be improved without significant impact on the healthy parts. Simulation study has been carried out to validate the feasibility and effectiveness of the proposed F2F AFC-bridge dc transformer. Moreover, its extensions to the generic multi-port configuration, bipolar arrangement and non-isolated dc auto-transformer concept can be derived accordingly [22-24, 28].

REFERENCES

[1] W. F. Long, J. Reeve, J. R. McNichol, M. S. Holland, J. P. Taisne, J. Lemay, D. J. Lorden, "Application aspects of multiterminal DC power transmission," *IEEE Trans. Power Del.,* vol. 5, no. 4, pp. 2084-2098, Oct. 1990.

[2] X. Wang and B. T. Ooi, "High voltage direct current transmission system based on voltage source converters," in *Proc. 21st Annu. IEEE Power Electron. Spec. Conf.,* 1990, pp. 325-332.

[3] A. Lesnicar and R. Marquardt, "An innovative modular multilevel converter topology suitable for a wide power range," in *Proc. IEEE PowerTech Conf.,* 2003, pp. 1-6.

[4] S. Debnath, Q. Jiangchao, B. Bahrani, M. Saeedifard, and P. Barbosa, "Operation, Control, and Applications of the Modular Multilevel Converter: A Review," *IEEE Trans. Power Electron.,* vol. 30, no.1, pp. 37-53, Jan. 2015.

[5] P. Bordignon, H. Zhang, W. Shi, N. Serbia, and A. Coffetti, "HV submodule technology based on press pack IGBT for largest scale VSC-HVDC application," in *Proc. 12th IET Int. Conf. AC DC Power Transm.,* 2016, pp. 1-6.

[6] N. Flourentzou, V. G. Agelidis, and G. D. Demetriades, "VSC-Based HVDC Power Transmission Systems: An Overview," *IEEE Trans. Power Electron.,* vol. 24, no.3, pp. 592-602, Mar. 2009.

[7] Z. Liu, J. Yu, X. Guo, T. Sun, and J. Zhang, "Survey of technologies of line commutated converter based high voltage direct current transmission in China," *CSEE J. Power Energy Syst,* vol. 1, no. 2, pp. 1-8, Jun. 2015.

[8] H. Atighechi, S. Chiniforoosh, J. Jatskevich, A. Davoudi, J. A. Martinez, M. O. Faruque, *et al.*, "Dynamic Average-Value Modeling of CIGRE HVDC Benchmark System," *IEEE Trans. Power Del.,* vol. 29, no. 5, pp. 2046-2054, Oct. 2014.

[9] M. Daryabak, S. Filizadeh, J. Jatskevich, A. Davoudi, M. Saeedifard, V. K. Sood, *et al.*, "Modeling of LCC-HVDC Systems Using Dynamic Phasors," *IEEE Trans. Power Del.,* vol. 29, no. 4, pp. 1989-1998, Aug. 2014.

[10] A. J. J. Rezek, A. A. d. S. Izidoro, J. S. d. Sa, and F. C. d. Fonseca, "The capacitor commutated converter (CCC) as an alternative for application in HVDC projects," in *Proc. IEEE Int. Symp. Ind. Electron.,* 2003, pp. 432-437.

[11] Y. Xue, X. P. Zhang, and C. Yang, "Elimination of Commutation Failures of LCC HVDC System with Controllable Capacitors," *IEEE Trans. Power Syst,* vol. 31, no. 4, pp. 3289-3299, Jul. 2016.

[12] P. Bakas, L. Harnefors, S. Norrga, A. Nami, K. Ilves, F. Dijkhuizen, and H.-P. Nee, "A Review of Hybrid Topologies Combining Line-Commutated and Cascaded Full-Bridge Converters," *IEEE Trans. Power Electron.,* vol. 32, no. 10, pp. 7435-7448, Oct. 2017.

[13] S. P. Engel, N. Soltau, H. Stagge, and R. W. D. Doncker, "Dynamic and Balanced Control of Three-Phase High-Power Dual-Active Bridge DC-DC Converters in DC-Grid Applications," *IEEE Trans. Power Electron.,* vol. 28, no. 4, pp. 1880-1889, Apr. 2013.

[14] R. W. D. Doncker and J. P. Lyons, "The auxiliary resonant commutated pole converter," in *Proc. IEEE IAS Annu. Meeting Conf.,* 1990, pp. 1228-1235.

[15] N. Soltau, H. Stagge, R. W. D. Doncker, and O. Apeldoorn, "Development and demonstration of a medium-voltage high-power DC-DC converter for DC distribution systems," in *Proc. IEEE Power Electron. Distrib. Gener. Syst. Conf.,* 2014, pp. 1-8.

[16] B. Zhao, Q. Song, and W. Liu, "Power Characterization of Isolated Bidirectional Dual-Active-Bridge DC-DC Converter With Dual-Phase-Shift Control," *IEEE Trans. Power Electron.,* vol. 27, no. 9, pp. 4172-4176, Sept. 2012.

[17] S. Allebrod, R. Hamerski, and R. Marquardt, "New transformerless, scalable Modular Multilevel Converters for HVDC-transmission," in *Proc. IEEE Power Electron. Spec. Conf.,* 2008, pp. 174-179.

[18] M. M. C. Merlin, T. C. Green, P. D. Mitcheson, D. R. Trainer, R. Critchley, W. Crookes, F. Hassan, "The Alternate Arm Converter: A New Hybrid Multilevel Converter With DC-Fault Blocking Capability," *IEEE Trans. Power Del.,* vol. 29, no. 1, pp. 310-317, Feb. 2014.

[19] G. P. Adam, S. J. Finney, B. W. Williams, D. R. Trainer, C. D. M. Oates, and D. R. Critchley, "Network fault tolerant voltage-source-converters for high-voltage applications," in *Proc. 9th IET Int. Conf. AC DC Power Transm.*, 2010, pp. 1-5.

[20] C. Oates and K. Dyke, "The controlled transition bridge," in *Proc. 17th Eur. Conf. Power Electron. Appl*, 2015, pp. 1-10.

[21] G. P. Adam, I. A. Gowaid, S. J. Finney, D. Holliday, and B. W. Williams, "Review of dc-dc converters for multi-terminal HVDC transmission networks," *IET Power Electron.,* vol. 9, pp. 281-296, Feb. 2016.

[22] G. J. Kish and P. W. Lehn, "A modular bidirectional DC power flow controller with fault blocking capability for DC networks," in *Proc. 14th IEEE Workshop Control Model. Power Electron.,* Jun. 2013, pp. 1–7.

[23] J. A. Ferreira, "The Multilevel Modular DC Converter," *IEEE Trans. Power Electron.,* vol. 28, no. 10, pp. 4460-4465, Oct. 2013.

[24] A. Schön and M. M. Bakran, "High power HVDC-DC converters for the interconnection of HVDC lines with different line topologies," in *Proc. IEEE Power Electron. Conf.,* 2014, pp. 3255-3262.

[25] G. P. Adam, S. J. Finney, and B. W. Williams, "Enhanced control strategy of full-bridge modular multilevel converter," in *Proc. Int. Conf. Renew. Energy Res. Appl.,* 2015, pp. 1432-1436.

[26] A. Nami, A. Hassanpoor, and Y. j. Häfner, "Theory to practical implementation of full-bridge modular multilevel converter for HVDC applications," in *Proc. 17th IEEE Int. Conf. Ind. Technol.*, 2016, pp. 378-383.

[27] G. P. Adam, K. H. Ahmed, and B. W. Williams, "Mixed cells modular multilevel converter," in *Proc. IEEE 23rd Int. Symp. Ind. Electron.*, 2014, pp. 1390-1395.

[28] P. Li, S. J. Finney, and D. Holliday, "Active-Forced-Commutated Bridge Using Hybrid Devices for High Efficiency Voltage Source Converters," *IEEE Trans. Power Electron.,* vol. 32, no. 4, pp. 2485-2489, Apr. 2017.

[29] C. Oates, K. Dyke, and D. Trainer, "The use of trapezoid waveforms within converters for HVDC," in *Proc. 16th Eur. Conf. Power Electron. Appl.*, 2014, pp. 1-10.

[30] T. Lüth, M. M. C. Merlin, T. C. Green, F. Hassan, and C. D. Barker, "High-Frequency Operation of a DC/AC/DC System for HVDC Applications," *IEEE Trans. Power Electron.,* vol. 29, no. 8, pp. 4107-4115, Aug. 2014.

[31] A. K. Jain and R. Ayyanar, "PWM control of dual active bridge: Comprehensive analysis and experimental verification," *IEEE Trans. Power Electron.,* vol. 26, no. 4, pp. 1215-1227, Apr. 2011.

[32] L. Qi, A. Antoniazzi, L. Raciti, and D. Leoni, "Design of Solid State Circuit Breaker Based Protection for DC Shipboard Power Systems," *IEEE J. Emerg. Sel. Topics Power Electron.,* vol. 5, no. 1, pp. 260-268, Mar. 2017.

[33] A. Nami, L. Jiaqi, F. Dijkhuizen, and G. D. Demetriades, "Modular Multilevel Converters for HVDC Applications: Review on Converter Cells and Functionalities," *IEEE Trans. Power Electron.,* vol. 30, no. 1, pp. 18-36, Jan. 2015.

[34] G. P. Adam and B. W. Williams, "Half- and Full-Bridge Modular Multilevel Converter Models for Simulations of Full-Scale HVDC Links and Multiterminal DC Grids," *IEEE J. Emerg. Sel. Topics Power Electron.,* vol. 2, no. 4, pp. 1089-1108, Dec. 2014.

[35] X. Jiang and M. M. Bakran, "A new protection scheme for HVDC circuit based on MMC topology with controllable fault current," in *Proc. 18th Eur. Conf. Power Electron. Appl.,* 2016, pp. 1-10.

[36] P. S. Jones and C. C. Davidson, "Calculation of power losses for MMC-based VSC HVDC stations," in *Proc. 15th Eur. Conf. Power Electron. Appl.,* 2013, pp. 1-10.

[37] T. Jonsson, P. Lundberg, S. Maiti, and Y. Jiang-Häfner, "Converter Technologies and Functional Requirements for Reliable and Economical HVDC Grid Design," in *Proc. CIGRE Canada Conf.*, 2013, pp. 1-9.

[38] B. Jacobson, P. Karlsson, G. Asplund, L. Harnefors, and T. Jonsson, "VSC-HVDC transmission with cascaded two-level converters," in *Proc. CIGRE Session,* 2010, pp. 1-8.